applied sciences

MDPI

Article

Manufacturing Process of Helicopter Tail Rotor Blades from Composite Materials Using 3D-Printed Moulds

Radu Torpan and Sebastian-Marian Zaharia *

Department of Manufacturing Engineering, Transilvania University of Brasov, 500036 Brasov, Romania; radu.torpan@student.unitbv.ro
* Correspondence: zaharia_sebastian@unitbv.ro

Abstract: Conventional processes require a mould for the manufacture of each test product, which often results in high costs but is ideal for large series of products. In contrast, for prototypes, additive manufacturing processes are a suitable low-cost time-saving alternative. The primary objective of this study is to investigate the capabilities of 3D-printed tooling in a real-life scenario for composite blades with low production numbers and prototypes in order to allow development and production costs to decrease and to also reduce lead times in the early phases of new projects. The 3D printing process is economically advantageous in terms of production costs for the composite blade mould, reducing the cost three times compared to the conventional manufacturing process. To obtain the composite helicopter blade, the following phases were carried out: the starting design of the mould, 3D printing and assembly of the mould sections, and blade manufacturing. The economic analysis of the two mould manufacturing methods shows an approximately equal ratio between the manufacturing costs of the 3D-printed mould and the manufacturing costs of the blade, whereas in the conventional processes, the costs for mould manufacturing represent 75% of the total cost and the rest (25%) of the cost is spent on blade manufacturing.

Keywords: manufacturing; tail rotor blade; composite; 3D printing; moulding; cost evaluation

Citation: Torpan, R.; Zaharia, S.-M. Manufacturing Process of Helicopter Tail Rotor Blades from Composite Materials Using 3D-Printed Moulds. *Appl. Sci.* **2024**, *14*, 972. https://doi.org/10.3390/app14030972

Academic Editor: Jérôme Morio

Received: 8 December 2023
Revised: 14 January 2024
Accepted: 22 January 2024
Published: 23 January 2024

1. Introduction

Helicopter blades are essential elements that can withstand high loads and, at the same time, need to be as light as possible. To meet these requirements, helicopter blades are manufactured using composite materials: carbon fibre, fibreglass, and Kevlar fibre [1]. In order for the helicopter blade to be used safely and with maximum efficiency, several structural criteria must be taken into account [2,3]: high resistance to forces in the axial direction, which is the main stress, as well as the secondary stress coming from the bending forces acting through the lift force generated by the aerodynamic profile of the blade and its angle of attack; low mass, which is necessary for two reasons: the first is the additional fuel consumption that the helicopter has to sustain to generate the force required to rotate the blades and the second is that through the action of the centrifugal force the mass effect of each fraction is amplified by at least one or two orders of magnitude, which further stresses the blade structure in the axial direction; and the fatigue strength of the material is also a very important factor as it is part of a dynamic assembly, the blade is constantly subjected to a load-unload cycle, which leads over time to fatigue cracks [4] and failure. The core of the helicopter blades [3] can be made of foam or a honeycomb structure (metallic, composite, and Nomex).

Composite materials are replacing the conventional ones (metals and wood) in the structure of helicopter blades due to their ease of processing and productivity. The main advantages of carbon fibre and fibreglass composites are the following [5,6]: high strength-to-weight ratio, excellent fatigue resistance compared to metal alloys, high strength, high corrosion resistance, and anisotropy (different physico-mechanical properties in different

directions). These properties are the main reasons for the use of composites in the manufacture of aircraft parts, which are improved performance resulting from the ability to optimise the shape, structure, and mechanical properties of the parts, and weight reduction, which improves the efficiency of the parts and the aircraft and allows a higher load or operating range for the aircraft [7].

Due to the fierce competition between companies, there is a desire to introduce superior products to the market in terms of operational performance, which can be achieved using accelerated reliability testing for blades [8] but also by determining reliability indicators for the spar structure of helicopter rotor blades [9]. An important aspect of helicopter maintenance and flight safety activities is the determination of blade life using fatigue stands and tests [3,10]. Fatigue is the process of localised, progressive, and permanent structural changes in one or more areas of the blade under stress that produce variations in stress and strain and may culminate in cracking or complete failure after a sufficient number of oscillations [11,12]. The vital components (blades) of the helicopter structure are subject to particularly rigorous testing, as they cannot be doubled and their failure can lead to serious accidents [13,14]. Another method used since the early stages of aeronautical products is finite element analysis (FEA). Various studies [15–17] determine the distribution of equivalent stresses and total displacements for helicopter blades made of composite materials by FEA. Another research direction dedicated to the study of helicopter blades is aerodynamic optimisation using neural networks based on CFD solutions [18]. In order to design blades with the longest life and the best stress resistance, engineers very closely analyse the behaviour of blades in service; therefore, non-destructive methods [19,20] and failure mode analysis [21,22] are current activities in the life cycle of aircraft parts.

The use of 3D printing in industry is particularly popular with TDVs (tools, devices, and verifiers) due to the fact that they are used for specific tasks, especially in the production of prototypes and single units of immediate need [23,24]. Thus, by using additive manufacturing processes, lead times are shortened and so costs decrease. This is possible because traditionally immediate-need TDVs are manufactured using computer numerical control (CNC) machines, which increase production and maintenance costs for this section that represents manufacturing preparation for a part/sub-part [25]. TDVs used in production that are currently suitable for additive manufacturing are represented by the following categories: templates for layout/marking [26,27], positioning/assembly devices [28,29], moulds for vacuum forming [30,31], moulds for injection moulding of plastics or vulcanisation of rubber [32–34], presses for bending thin sheets [35–37], and moulds for making composite parts [38–40].

The moulds used for the production of composite parts have developed with the evolution of additive manufacturing processes and are mainly used in processes and technologies that operate at low temperatures and pressures. Given the high cost of a mould made by conventional processes, additive manufacturing processes are an alternative that reduce cost and production time due to the flexibility of parts that can be manufactured using 3D prototyping [41].

An important direction of research is the production of composite blades using different methods of manufacturing using moulds. In a recent study [42], a composite blade of the tail rotor of the IAR330 helicopter was designed and analysed using the finite element method. This blade was manufactured, at a scale of 1:3, from carbon-roving spar embedded with epoxy resin, a 3D-printed honeycomb core, and an outer skin made by hand lay-up of multiple carbon-fibre-reinforced laminae; the major advantage of manufacturing this kind of blade is the low cost.

Dippenaar et al. [43] manufactured a wind turbine blade, made of carbon fibre, using the vacuum-assisted resin transfer moulding (VARTM) process and a 3D-printed mould. The main contributions of the study are the technical evaluation of the process and a cost model for 3DP moulds for VARTM that can be used to assess the feasibility of the process. It was also observed that the 3D print tooling is less accurate compared to tools made on CNC but that there is a cost and time advantage to making tooling with 3D printing

processes. The life of the 3D-printed mould is limited to 15 to 30 parts, as significant wear occurs in the manufacturing process [43].

Bell and Ingersoll Machine Tools companies partnered to additively manufacture a long vacuum trim tool used to produce rotor blades for helicopters, using a hybrid machine that combines 3D printing and 5-axis milling [44]. A partnership of the US Department of Energy's (DOE) Oak Ridge National Laboratory (ORNL), National Renewable Energy Laboratory (NREL), Sandia National Laboratories, and private company TPI Composites demonstrated the feasibility of manufacturing wind turbine blades using 3D-printed moulds, highlighting the reduced manufacturing time and cost of these tools [45].

In this paper, the feasibility of the process of manufacturing a composite helicopter blade using a 3D-printed mould was demonstrated. To obtain the composite helicopter blade, all the necessary steps were carried out, starting from the design of the mould, 3D printing and assembly of the mould sections, and blade manufacturing; finally, a comparative study was carried out on the costs of manufacturing a 3D-printed mould and the costs of a CNC manufactured mould.

2. Mould Design

For the design of the mould needed to manufacture the IAR 330 helicopter anti-torque rotor blade from composite materials, several factors must be established regarding the operation of this part. When the design phase of the mould starts, it is important to know the role and the way the blade is used in operation, so that the most appropriate decisions can be made regarding the manufacturing method taking into account the practical use.

For the manufacture of the mould, two manufacturing processes have been analysed, so the process can be customised for the project in question (blade), which leads to a structural solution superior to the one chosen without a prior study of the existing documentation. The manufacturing of the moulds used is carried out by conventional milling processes, which can make it difficult to obtain the air foil in areas of high interest, with these areas being the air foil edges (leading and trailing).

One of the methods considered is conventional moulding in which the anti-torque blade is manufactured using two moulds (upper and lower) that make up the blade profile. To these, the following blade parts are added: the spar, made of roving fibres; the core made by machining; and the shell, which is assembled in the mould and cured under pressure in an autoclave. Although it is a faster process in terms of the moulds and tools used, this type of manufacturing requires external pressure and the presence of a vacuum in order to be carried out. The control of the composite materials used in the technological process is not 100% possible because once the mould is closed there is no definitive certainty that each start is in the position in which it was originally placed, which can result in ridges in the surface of the shell or bending of the whole assembly [46].

In the second method, the main spar of the blade is made with a vacuum and the shell and supporting structure are added separately by bonding and lamination. With this method of manufacturing and moulding, the quality and dimensional control of the blade parts can be much better monitored and controlled, resulting in a higher overall quality of the finished product. A disadvantage of this manufacturing method is that it requires three distinct types of moulds: one for manufacturing the blade spar, one for manufacturing the shell, and one for manufacturing the composite assembly, assuming that the material used for the insert is machined or prefabricated by extrusion beforehand. This method is therefore also costly and time-consuming due to the large number of TDVs required to manufacture the part. The big advantage is to obtain a hollow inner cavity, which reduces the total mass of the blade. The structural stiffness of this structural solution is high due to the fact that the moment of inertia area of the spar section is increased by the arrangement of composite material fibres at the edge of the blade geometry [47].

The helicopter blade (Figure 1a) is made up of two types of geometric sets, the first geometric set (monoblock area—Figure 1b) refers to the area where the blade is embedded in the rear rotor hub of the aircraft and is intended for the blade embedment and transmission

of the lift force. The second geometric set (constant chord area—Figure 1c) is the lifting structure, which plays a role in creating the desired aerodynamic effect.

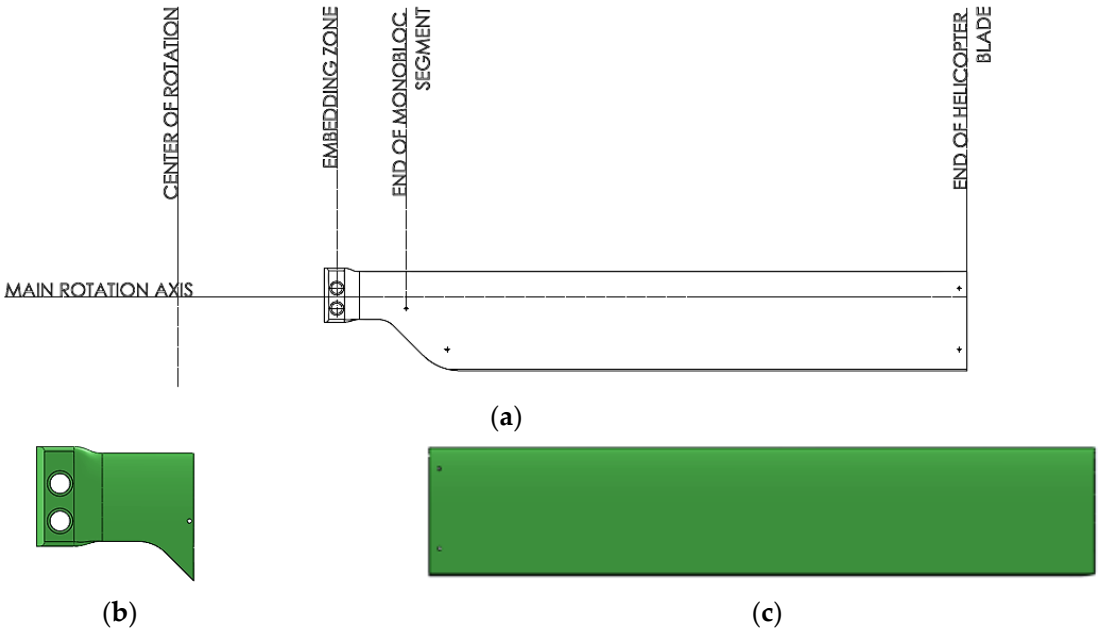

Figure 1. Helicopter blade shape. (**a**) The main axes of construction of the anti-torque blade. (**b**) The monoblock construction section of the blade. (**c**) Constant section of the blade with NACA 0012 air foil.

Of particular importance from the point of view of manufacturing preparation is the achievement of the tolerances required by the product (blade). The following two general types of tolerances must be met:

1. Form tolerances—these are important because each manufactured blade must comply with the interchangeability scheme established for the aircraft, so the mould must be designed so that surface fit and deburring are minimised;
2. Dimensional tolerances—these serve to position the blade parts as accurately as possible. Additional elements such as steel bushings, dynamic balancing masses, or foam inserts are embedded in the composite material by means of moulding. Usually, from this point of view, the mould is made to a tolerance of half the tolerance [48] of the part (e.g., a tolerance of +0.1 mm is provided for the distance between the axes of the embedding bores; therefore, this dimension in the case of the mould will be tolerated +0.05 mm).

The geometry of the structure that serves to embed the blade in the rear rotor hub is suitable for a monoblock solid lamination made of a composite material chosen by the product designer. Thus, this section should be made using a compression mould, with such moulds being able to obtain complex solid geometries. The second section of the blade is geometrically constant, so after the connecting section between the two bodies, the body with a constant aerodynamic aerofoil is created. This blade section can be produced using conventional moulds or compression moulds.

In conclusion, the compression moulding option is chosen for the manufacture of the blade, as this option offers good possibilities for fast manufacture and ease of the digital model design. The geometry of the anti-torque blade allows the manufacture of a mould with a single separating plane, thus resulting in a mould consisting of two moulds: an upper one and a lower one. The lower mould acts as a loading area for the laminating materials and the upper mould acts as a punch. The punch, once assembled, is used to create the geometry on the upper surface of the blade and during the compression of the laminate composite, it evacuates the air and excess resin that has been added during the

lamination process. The compression carried out by the mould punch also presses the layers of the composite material so that the volume ratio between fibres and reinforcing resin is approximately 50% composite fibre and 50% reinforcing resin. This is particularly important in manufacturing the blade to ensure resin impregnation throughout the volume of the fibres that does not contribute structurally to the stiffness of the blade, without adding resin mass.

The design of the lower mould construction is to create a cavity deep enough to allow for the arrangement of the blade materials. Thus, the geometry of the lower surface of the blade is carried out in the body of the mould. Additional processes are added to the inner vertical walls of the mould to allow the extraction of the punch after curing and to facilitate the removal of the blade. Thus, in the case of the lower mould, the draft angle of the inner walls was 5°. The main aspect of the design of TDVs for this manufacturing process is to include a telescopic section, where the upper mould acts as a punch in a cylinder during its closing. This allows the uncompressed fibres to be filled in and during closing the excess resin will be squeezed out through the separation line; but, due to a tight fit, the fibre cannot be removed, leaving the correct fibre to resin ratio. This telescoping element or punch must be deep enough to allow the mould to start closing before disrupting the fibre. The exact size of this element varies depending on the shape and design of the mould but, generally, it should extend to at least 25% of the depth of the final part. In the case of a two-part mould, this requires a draft angle of 3–5 degrees to allow easy separation of the mould.

In order to allow easy and unambiguous identification in both the design and the tracking and implementation process, the two moulds will be named as follows:

- The female (lower) mould or the mould into which the fibres have been loaded is named MAT-COMP V3-FEMALE (Figure 2a);
- The male mould (upper) or the mould which compresses the composite material after lamination is called MAT-COMP V3-MALE (Figure 2b).

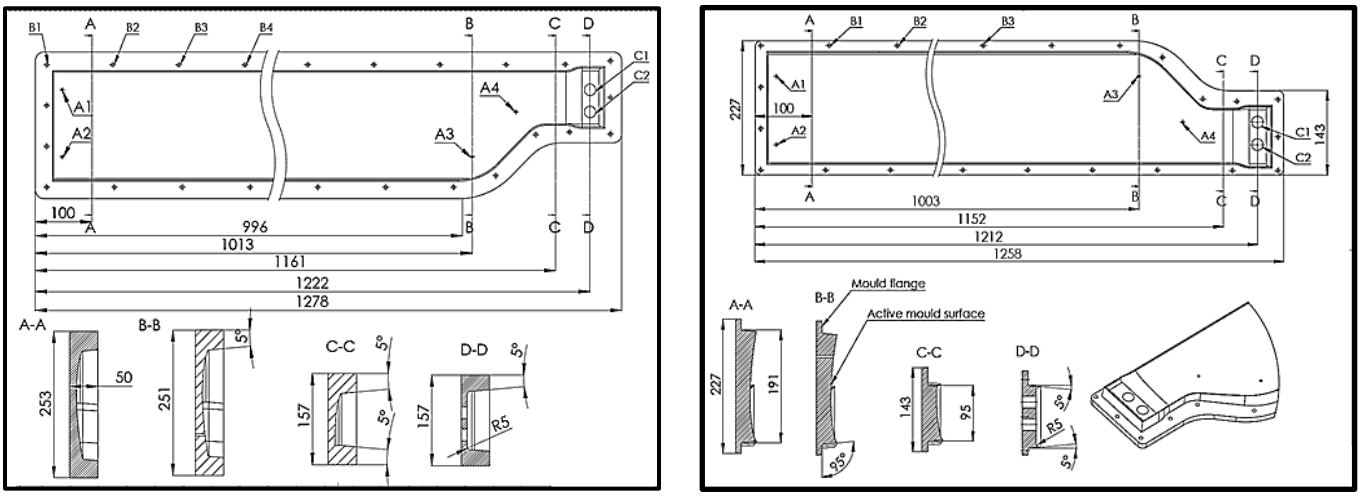

(**a**) (**b**)

Figure 2. Helicopter blade mould drawing (dimensions in mm). (**a**) Lower mould (MAT-COMP V3-FEMALE). (**b**) Upper mould (MAT-COMP V3-MALE).

The lower mould (Figure 2a) has three types of bores in its body, which are used to assemble and position the fixing and extraction elements after polymerisation. These types of bores are not essential in the manufacturing process but with their help, the yield of the mould is greatly increased due to the much more efficient guiding of the two moulds when closing them. The first set of bores is used to position the blade core in the mould and to fix it in position. At the same time, the clamping rods that go into the bores also act as extractors once the anti-torque blade has been laminated and the curing process is complete. These bores are shown in Figure 2 and are numbered alphanumerically as A1,

A2, A3, and A4. The positioning of these bores allows the application of the extraction forces to be distributed close to the vertical walls of the mother mould, to corners, or to geometric surfaces that are difficult to extract, for example, the tip of the blade area and the blade embedment area. The second set of bores, B1, B2, and B3, is used for the assembly parts (screw shank) that are arranged around the blade contour and their purpose is to provide the necessary compression force to the punch to remove the excess resin. Their diameter is 8.2 mm and the assembly is carried out with a clearance fit. This increased tolerance ensures that each screw can be assembled and take up the deviations from the 3D printing process of the mould. The C1 and C2 bores have a diameter of 20 mm and, by means of two polyamide rods, place the embedded metal bushings in the embedded tip of the composite blade. In other words, the positions of the C1 and C2 bores determine the centre of the axis of the bolts that assemble the blade to the rear rotor hub, so the tightest tolerance in the whole mould assembly can be found here, which is ± 0.02 mm.

The upper mould (Figure 2b) is manufactured from a punch, which has the active surface machined according to the geometry of the upper surface of the blade, in order to shape the laminated composite in the mould. The 5° draft angle is added to this surface, also present on the surface of the lower mould, and the upper part of the male mould ends with a clamping flange that will ensure pressure on the freshly laminated blade. A similar system of B bores is found in the flange of the upper mould and allows the passage of the screw shank, thus allowing the mould to close. The positioning A bores are present in the body of the upper mould but, unlike the lower mould, they serve only to position the rods guiding the anti-torque blade core. The extraction from the punch is not necessary in this case. The positioning of the polyamide rods securing the metal bushes embedded in the composite is performed similarly to the lower mould. It is important to mention the concentricity condition to be met by the C1 and C2 bores used in the two moulds. This condition of concentricity actually ensures the perpendicularity of the axes of the embedded metal bushes to the plane of symmetry of the composite blade, which is essential in future measurements and checks that the blade has undergone the appropriate steps before it is mounted on the helicopter. Another important aspect is that after lamination, the axes of the embedding bushings are considered as reference points and starting points for future operations as well as for their mounting on the aircraft.

For a better understanding of the manufacturing process of the anti-torque blade, the assembly and operation of the mould are further described. The design of the mould would be incomplete without describing the plan of the operations that are carried out with it. In fact, it is at this stage that the set of TDVs required for a lamination operation begins to become clear. The lower mould placed with the active area upwards on the workbench is equipped with guide rods for the blade insert and guide rods for the steel bushes to be embedded in the blade. Notably, the assembly between the guide rods is made with slide clearance as follows: H7/g6, so that the required geometric tolerance can be ensured. The next step in the assembly is the fitting of the metal bushes into the mould, followed by the closing of the mould by placing the upper mould on top, moving it in the Z direction ensures the closing. Guiding of the upper mould at the time of closing is achieved by means of guide rods (position 4 in Figure 3) and vertical walls in which the draft angle has been included. The mould is then assembled with M8 $\times$ 80 screws and clamping is carried out until the upper mould flange is in contact with the lower mould (Figure 3).

For high-volume manufacturing, compression moulding tools for this process are usually made of aluminium or steel machined by milling. These obviously offer excellent strength and durability but are expensive to produce, making them less viable for small series and prototypes.

Design parameters taken in consideration for the mould of the anti-torque blade are as follows (Table 1): volume to be filled by layup process, cavity design, and clamping force required in order to evacuate the excess resin, geometrical dimensions, tolerances, and part removal when the curing process is finished.

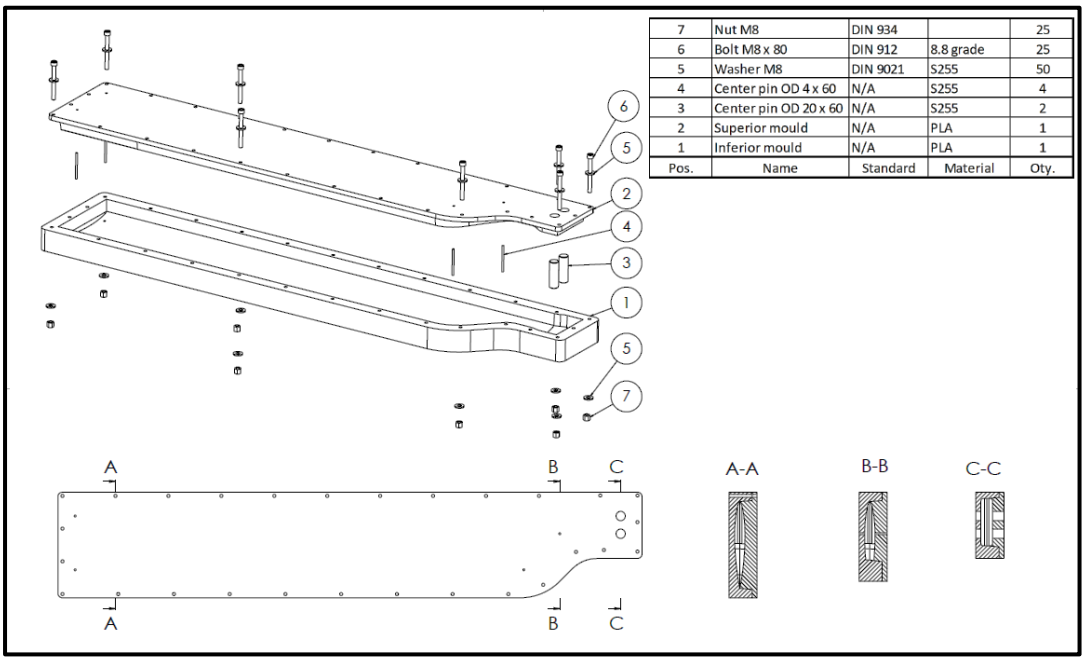

Figure 3. Mould assembly drawing.

Table 1. Mould design parameters.

Process Parameters	Value
Volume filled [dm^3]	3.38
Cavity design	Open
Clamping force [Nm]	20
Mould tolerance [mm]	±0.2
Ejector system	Rod type
Moulding temperature [°C]	20
Moulding pressure [bar]	20
Fibre to resin ratio [%]	60–40
Compression time [h]	48

For the design of the 3D-printed mould, the following aspect was also taken into account: the minimum wall thickness should be at least 3 mm and cores with thick sections should be used to prevent thermal cracking due to curing and mould damage due to high exotherms [43,49,50].

3. Three-Dimensional Printing of the Mould

In this study, the direct 3D-printed TDV moulding method was used with the Ultimaker S5 printer (Ultimaker, Utrecht, The Netherlands). Although this 3D-printed mould does not offer the strength and durability of conventional moulding tools, it has the advantage of being very cheap, fast in manufacturing, and very useful for small series and prototypes. Using this method with a 3D-printed mould allows the production of parts with very high mechanical performance without the need for additional specialised equipment or tools. Although other types of filaments can also be used, polylactic acid (PLA) has been found to offer high precision, low shrinkage, and ease of printing, making it an excellent choice for mould making [51–53].

The affordable cost of PLA is still a determining factor in choosing it for mould making. Compared to filaments made from acrylonitrile butadiene styrene (ABS) or nylon, the filament made from PLA is about 20% cheaper than these. This makes it a suitable choice for moulds that require a large amount of material but for projects that do not have a large budget. The environmentally friendly and sustainable aspect of PLA is due

to the fact that it is made from renewable raw materials such as corn or other plants, making it an environmentally friendly material. PLA production generates lower CO_2 emissions and uses less energy than petroleum-based materials such as ABS. PLA is also biodegradable, which means that it can be broken down naturally by microorganisms in the environment [54]. This characteristic makes PLA a suitable choice for applications that require minimal environmental impact [55].

In order to manage the 3D printing of a mould that exceeds the printing dimensions of the 3D printer in the X and Y directions, an alternative solution was needed to divide the mould into smaller sections that can be printed separately. However, a major drawback associated with this method is that once the initial mould geometry is split, the accuracy of the mould decreases along the direction in which it is split. To compensate for this problem and to ensure a correct and accurate assembly of the resulting mould from individual sections (Figure 4a), a puzzle-type assembly (Figure 4b) was chosen.

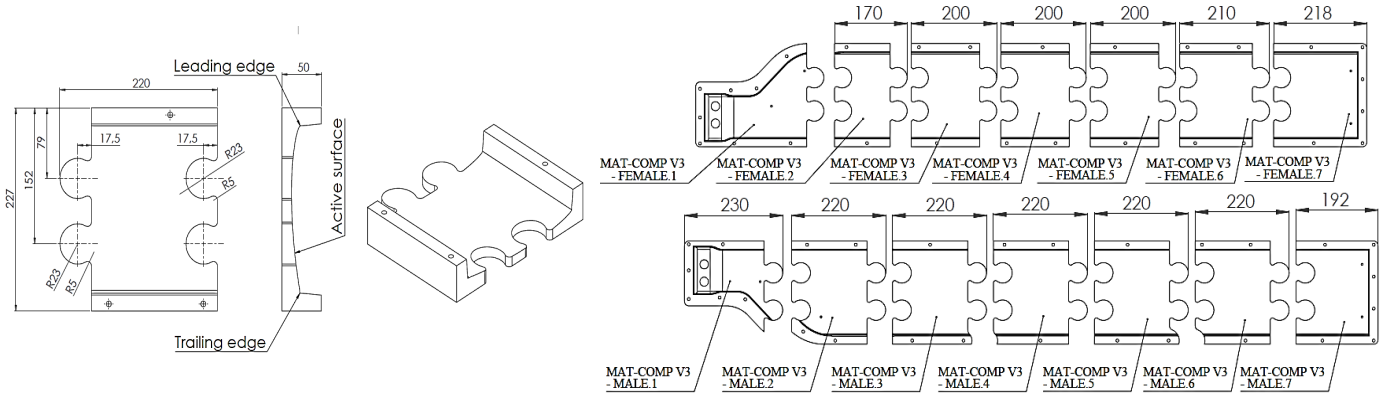

(**a**) (**b**)

Figure 4. Mould design (dimensions in mm). (**a**) Section 3 (MAT-COMP V3-MALE). (**b**) Preparing the mould sections for 3D printing.

Due to the geometry of the cylindrical section and similar dimensions there is a risk of mixing up sections within the same mould. To combat this risk, each part is marked as shown in Figure 4b. This also ensures the correct assembly of the moulds and the alignment of the fixing and assembly bores. By using this assembly method, each section of the mould can be accurately and securely positioned and clamped, ensuring the correct geometry and stability of the final mould. It is essential that the assembly process is well planned and that each part fits perfectly into the puzzle template, avoiding discrepancies or clearances that could affect the final mould. This approach offers a practical and efficient solution for 3D printing large-sized moulds using a 3D printer with limited capacity. Precise mould splitting and assembly allows large moulds to be manufactured affordably and efficiently without compromising the quality and accuracy of the final mould.

The choice of the sectioning areas is made by taking into account two important design parameters in terms of the structural integrity of the mould, as follows:

- The first aspect considered is the size of the printing bed plate because after trials and tests it was concluded that by making a section for printing using the maximum printing bed plate size (330 mm × 240 mm), the marginal geometry was made with poor geometrical tolerances and questionable structural integrity. As a result, the size of the 3D printer bed plate was taken as a reference, 240 mm × 240 mm, for dividing the sections of the two moulds (upper and lower);
- The second aspect is related to the integration of the bores present in the mould in the same printed section. The decision was taken not to split a bore between two 3D-printed sections. By doing so, each section of the moulds can work independently when assembled and they are responsible for the cross-sectional result of the

anti-torque blade. The overall assembly of the mould was responsible for supporting the sections and arranging them rectilinearly.

The CAD model sections of the mould were saved in STL (stereolithography) format to be imported into the Ultimaker Cura 4.13.1 manufacturing preparation software system (Ultimaker, Utrecht, The Netherlands). The manufacturing parameters for the PLA filament of the 3D printing process for the mould sections are presented in Table 2. The high thickness of the outer walls of the sections, as well as the infill density of 30% with an infill pattern grid, ensures superior mechanical behaviour, so the mould can withstand the stresses that develop when it is closed.

Table 2. Three-dimensional printing parameters of the mould sections.

3D Printing Parameter	Value
Filament	UltiMaker PLA white
Filament diameter [mm]	2.85
Layer height [mm]	0.2
Wall thickness [mm]	3
Wall line count	10
Top/Bottom layers	12
Infill density [%]	30
Infill pattern	Grid
Print speed [mm/s]	90
Travel speed [mm/s]	130
Printing temperature [°C]	200
Building plate temperature [°C]	60
Nozzle diameter [mm]	0.4

In Figure 5a,b, the positioning of the mould sections on the building plate from the software system for preparation for manufacturing was described and finally, a section made by the 3D printing process can be observed.

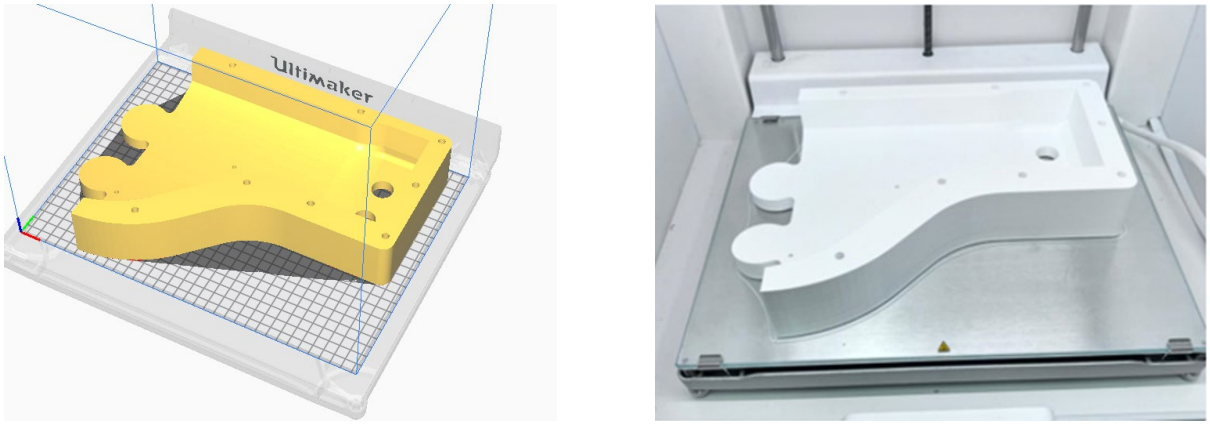

(**a**) (**b**)

Figure 5. Manufacture of the mould sections. (**a**) Preparation for 3D printing of the mould sections. (**b**) Printed Section 3D of MAT-COMP V3-MALE1.

The 3D printing time and filament consumption involved in the manufacturing of the anti-torque blade mould, as presented in Table 3, show the size or the order of magnitude of the working time required, as well as the material consumption. Thus, the manufacture of the MAT-COMP V3-FEMALE sections took 254 printing hours and used 572.44 m of filament or approximately 4.5 kg of PLA filament. The sections of MAT-COMP V3-FEMALE were manufactured in 248 printing hours and used 615.86 m of filament or approximately 4.8 kg of PLA filament. Finally, the 3D printing of the upper and lower mould sections took 502 h, consuming 1188 m of PLA filament and 9.3 kg of PLA filament. To reduce the time

of manufacturing the mould, an efficient option could be the use of the 3D print farm. This production line, formed by a group of 3D printers that manufacture simultaneously and as much as possible without stopping, aims to increase the production rate of printed parts.

Table 3. The printing time and filament consumption needed to manufacture the anti-torque blade mould.

Mould	3D-Printed Section	Manufacturing Time [h]	Filament Consumption [g]	[m]
MAT-COMP V3-FEMALE	1	49	874	110.52
	2	27	473	59.8
	3	33	578	73.08
	4	33	578	73.03
	5	32	575	72.7
	6	34	616	77.82
	7	46	834	105.49
SUBTOTAL MAT-COMP V3-FEMALE		254	4528	572.44
MAT-COMP V3-MALE	1	49	874	110.52
	2	32	653	82.56
	3	34	678	85.75
	4	33	637	85.07
	5	34	686	86.71
	6	33	667	84.26
	7	33	641	81.02
SUBTOTAL MAT-COMP V3-MALE		248	4836	615.89
TOTAL		502	9364	1188.33

4. Composite Blade Manufacturing

After the sections of the two moulds are 3D printed (Figure 6a), they are assembled using a rubber hammer and a polyamide punch and placed on a flat plane. The sections are bonded together (Figure 6b) using a polyurethane adhesive, which has the advantage that as it hardens, the volume of the adhesive increases, thus ensuring the tightness of the mould and filling any gaps that may occur. The assembly of the mould is followed by the adjustment of the active surfaces. These are sanded and, where necessary, filled with putty to fill in low areas and even out the surface. Next, the mould is coated with a layer of 2K primer (Figure 6c), which serves as a separation layer between the composite (blade) and the 3D-printed mould.

The manufacture of the anti-torque blade begins with the preparation of the parts that are to be used and the preparation of the moulds. Thus, the first step is to manufacture the blade core by 3D printing (Figure 6d). To do so, the following were of great importance: the walls should be as thin as possible and the infill density as low as possible. The blade core takes the place of a structure for which traditionally, various materials are used [56,57], namely PVC foam (polyvinyl chloride), moltoprene, Nomex honeycomb, and metallic honeycomb. The advantage of a 3D-printed core allows the construction of a hollow cavity which decreases the overall mass of the finished part. The core is manufactured on a Prusa MK2 3D printer (Prusa Research a.s., Prague, Czech Republic) from PLA filament, it has an outer wall of 0.3 mm and 4 inner stiffening ribs of the same thickness (Figure 6d); additionally, it has two perforated bores allowing the insertion of carbon rods.

As shown in Figure 6e, the anti-torque blade is built from the outside to the inside from a carbon fibre shell, which encloses a structural box girder made of two unidirectionally-arranged fibreglass spars, the direction of lamination being in the blade span. In the mid-section, the blade box girder is made up of a 3D-printed core through the middle of which two 4 mm diameter carbon rods pass. These rods are used to join the core structure, which is made up of six sections. The tips of the rods are inserted into the end section of the blade core and pass through the perforated bores of the core. These rod tips are embedded in the carbon section called the monoblock section of the blade. Additionally, after the

lamination of the monoblock structure, two layers of Kevlar are laminated to the leading edge. The Kevlar layers are added for reinforcement of the structure in case of impact or to prevent premature wear of the blade.

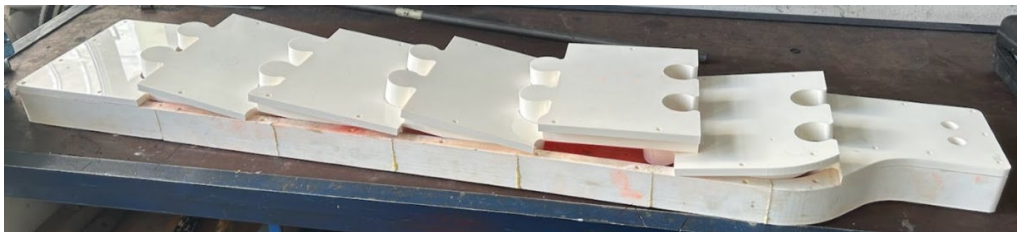

(**a**)

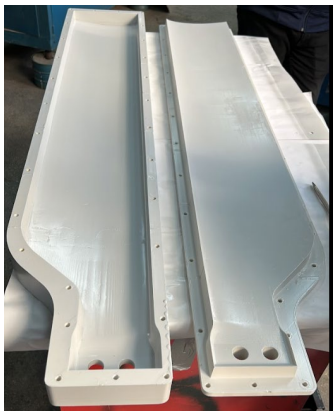

(**b**)

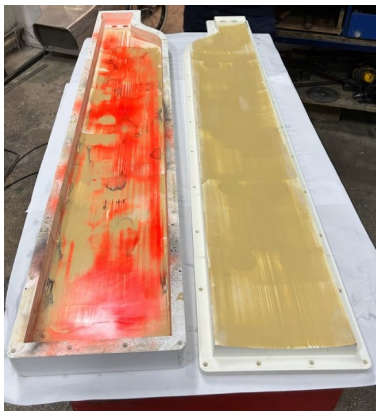

(**c**)

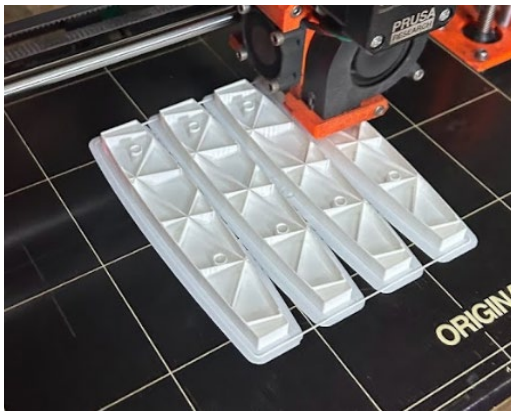

(**d**)

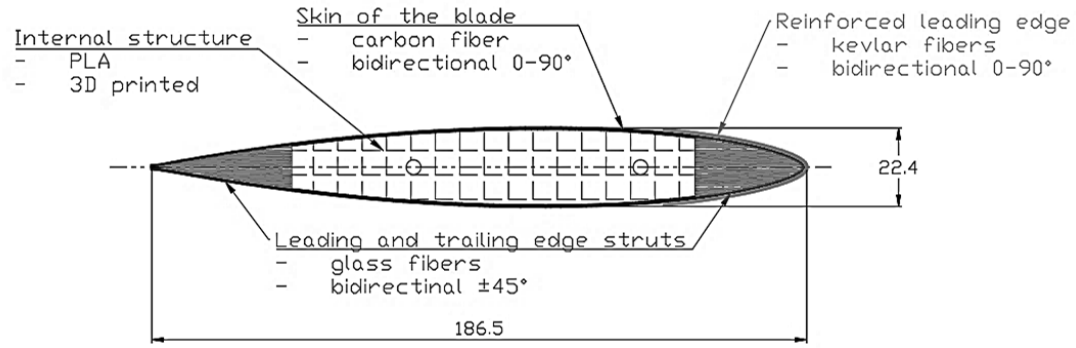

(**e**)

Figure 6. Assembly of the printed mould 3D. (**a**) Printed sections 3D. (**b**) Assembly of the mould for the anti-torque blade. (**c**) Priming of the working area of the 3D-printed mould. (**d**) Three-dimensional printing of the blade core. (**e**) Cross-section of the anti-torque blade with an indication of materials and layout areas (dimensions in mm).

In order to obtain a roughness of the active surfaces of the two moulds (upper and lower), two models of the upper surface (Figure 7a) and lower surface (Figure 7b) of the blade were manufactured by the thermoplastic extrusion process, this time being positive shapes of the mould section. The active surface of the mould is sanded with the help of these and abrasive paper of different grits. The grits of the abrasive paper used are in ascending order as follows: 120, 180, 240, 320, 480, 600, and 1000 (note that the sanding for grits of 480 and above was conducted in the wet condition).

(**a**) (**b**)

Figure 7. Digital model required for mould sanding: (**a**) upper mould template and (**b**) lower mould template.

As shown in Figure 8a, after 3D printing and assembly of the core, it is inserted into the mould for a final trial run for the geometry to be used further and to make the necessary adjustments. In order to control the position of the core inside the mould as precisely as possible, four centring studs are used (Figure 8b), which are arranged as follows: two at the distal end of the core and two at the proximal end of the core (Figure 8c).

(**a**) (**b**) (**c**)

Figure 8. Centring the core in the mould. (**a**) Distal end. (**b**) Proximal end. (**c**) Lower mould-positioning of the blade core.

Once the core is made, the next step is to cut the layers of material that make up the anti-torque blade. The layers are cut according to the draping diagram. The draping diagram is usually specified in the design drawing of the part and specifies the type of layers (fibreglass, carbon fibre, Kevlar, etc.) found in the composition, the density of the layer per square metre (200 g, 300 g, 600 g, etc.) their size (cutting dimensions), the orientation or positioning of the layers on the part in relation to the main axis of the part, and the order in which they are laid down.

Next, five successive layers of wax are applied to the surface of the two moulds to create a separating film between the composite blade and the 3D-printed mould. These wax layers are intended to make it easier to remove the blade from the 3D-printed mould after the polymerisation process is complete. The layers are applied sequentially with a strip of fabric at 15 to 20 min intervals between applications to allow the layers to adhere to the moulds and to each other.

Layer cutting is performed by hand, using scissors specially designed for fabric-type products. This is how the layers are cut.

The fibres that are part of the blade are as follows:

1. Carbon fibre fabric 2 × 2 twill 3K with a weight of 200 g/m^2 [58]: six layers are cut to form the blade shell and three layers are placed on the lower surface and three layers are placed on the upper surface;
2. Fibreglass fabric, with a weight of 200 g/m^2 [59], is cut as follows:
    - For the spar constituting the leading edge of the blade (Figure 9), about 75 layers are cut, ranging in width from 5.5 mm to 31 mm. The variation in layer width is necessary to form the specific shape of the leading edge.
    - Approximately 50 layers of varying widths between 5.5 mm and 40 mm were required for the spar constituting the trailing edge (Figure 10).

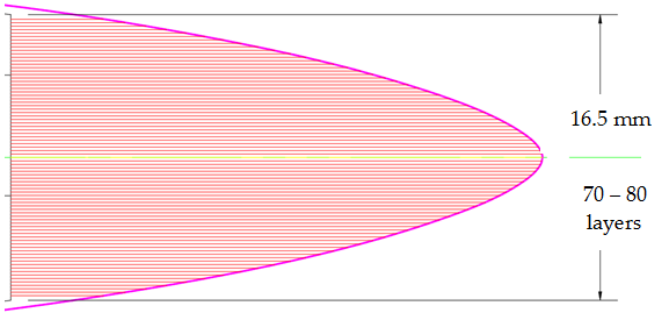

Figure 9. Cutting the layers of the spar constituting the leading edge of the blade.

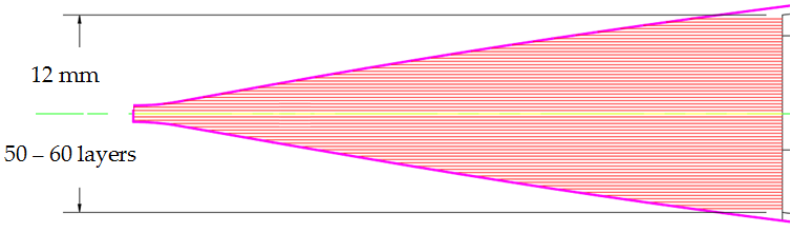

Figure 10. Cutting the layers of the spar constituting the trailing edge.

3. Short fibres:
   - made of Kevlar: they are obtained by cutting a Kevlar fibre fabric with a weight of 300 g/m^2 [60];
   - made of carbon: they are obtained by the same process as the fabric shown in Section 1 (carbon fibre fabric with a weight of 200 g/m^2).

Together, the short fibres form the monoblock section or the blade embedding section. The total volume of this section is 288.38 cm^3. The Kevlar to carbon ratio in this section is 50–50%.

4. The resin used is an epoxy resin—EL2 [61]—with AT30 fast hardener [62]. A total of 1000 g epoxy resin is used for the composite blade. The resin utilized in the manufacturing process of the anti-torque blade is divided into four batches. Epoxy resin is prepared on demand as needed for layup. The time elapsed between the first and last batch of resin is 100 min. After the layup process is finished and the two halves of the mould are closed, the composite blade is left to cure at room temperature, 20 °C.

The actual lamination of the blade begins with the application of a layer of epoxy resin in the lower mould (MAT-COMP V3-FEMALE) which actually prepares the application of the first layer of carbon. Three consecutive layers of carbon are applied to form the lower section of the blade shell (Figure 11a). These are followed by the insertion of the studs for positioning the core in the mould, followed by the insertion of the 3D-printed core (Figure 11b). At this stage, the centring studs, made of polyamide, of the metal bushings that will be embedded in the composite are also inserted. The centring studs are also used to position the metal bushes in their final position in a similar way to fixing the 3D-printed core.

After the core is positioned in the mould, the leading and trailing edge spars are manufactured, thus forming the blade girder box. The fibres of the spars are arranged along the 0° direction of the blade, i.e., along the blade. The leading-edge spar comprises 32 layers of fibreglass arranged longitudinally and the trailing edge spar comprises 27 layers of fibreglass (Figure 11c). In order to prevent the layers of fibreglass from clumping or having ridges, the width of the layers laid in the mould varies directly in proportion to the width inside the mould. Thus, the first layers are the narrowest, then their width increases

progressively up to the middle of the blade after which they progressively decrease in width until the last layer, which, similarly to the first layer laid, will be the narrowest.

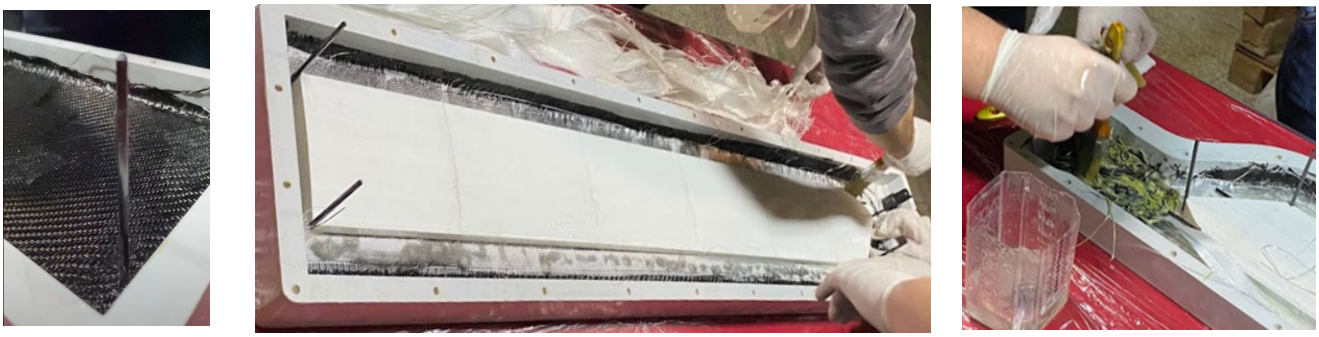

(**a**) (**b**) (**c**)

Figure 11. Blade manufacture. (**a**) Lamination of the lower blade shell. (**b**) Fitting of core guide studs. (**c**) Laminating the monoblock area and embedding the layers composing the blade spars in the monoblock area.

In parallel with the lamination of the leading edge and trailing edge, the blade embedment area or monoblock area, as it has been called during this work, is also laminated. The monoblock, being composed of short carbon and Kevlar fibres, is laminated in parallel with the lamination of the spars in order to interleave the unidirectional fibreglass within this structure, thus establishing the functional link between the two types of geometries, the variable and the constant.

The last operation in the stage of loading the mould with material consists of adding the layers that make up the upper blade shell. Three layers of carbon fibre are added, as in the case of the lower shell, which cover the constant section of the blade and continue onto the variable geometry section. This step is followed by the laying of the punch and the upper mould (MAT-COMP V3-MALE) over the lower mould (Figure 12a). After laying, the punch is lightly pressed to allow the resin to impregnate all fibres that are not saturated. The screws are positioned in the bores on the mould edges and the closing stage is started (Figure 12b).

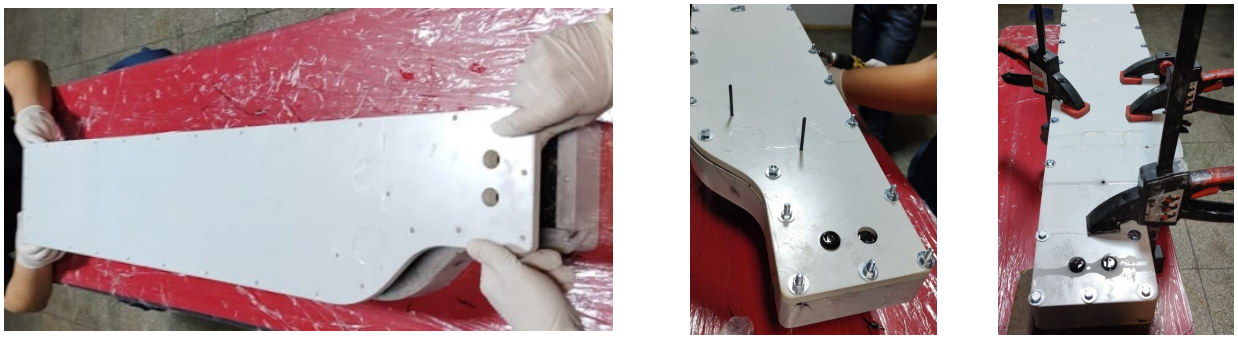

(**a**) (**b**) (**c**)

Figure 12. Blade manufacture. (**a**) Closing the mould after blade lamination. (**b**) Clamping the two moulds. (**c**) Use of compressive force to remove excess resin.

This stage begins with tightening, but not to the final torque, of the screws at the distal end of the blade towards the proximal end (towards the embedment). This type of tightening allows the excess resin to move towards the area where the most fibres are present, thus ensuring full impregnation. After the intermediate tightening of the screws, following the same assembly sequence, the screws of the two moulds are tightened to the final torque while also ensuring contact between the flange of the upper mould and the flange of the lower mould (Figure 12c). In this state, the composite blade is left to cure

for 48 h. For open surface application, the curing time of the resin used is 24 h but since curing takes place in a closed enclosure, double the time is allowed to compensate for the possibility of a delay in the curing process.

After this time, the mould screws are loosened and extracted. Wedges are inserted between the flange of the upper mould and the lower mould and a rubber hammer is used to separate the two moulds. This stage is followed by the removal of the blade from the mould. Extraction is carried out using rods and bores that were previously used to position the 3D-printed core. It is worth noting that during the demoulding process, the anti-torque blade is extracted from the lower mould (MAT-COMP V3-FEMALE). After the extraction of the anti-torque blade, the resulting rough sample is mass evaluated by weighing, resulting in a mass of 2116 g before deburring. The next step is the adjustment of the sample by removing the burrs resulting from the lamination process. The adjustment is carried out mechanically using a cutter and abrasive paper. The thin edges (less than 0.3 mm) are removed with the cutter and the finishing of the leading and trailing edges is completed with sandpaper, progressively increasing the paper grain size from 80 to 240.

With the help of a bench vise, the blade is embedded using a fixture in the provided bores (the same bores in which it is embedded in the tail rotor hub). In this assembly, the finishing carbon layers as well as the Kevlar fibre layers are applied (Figure 13a). The role of the red 2 × 2 twill 3K carbon fibre layers [63], with a weight of 210 g/m^2 (Figure 13b), is to increase the visibility of the blade during operation of the helicopter, thus reducing the risks associated with injury to aircraft crew during operation (Figure 13b). This type of safety measures is mainly used in aerospace systems such as helicopters, aircrafts, and light aircraft where the disc formed by the blade during operation of the powerplant (or propeller) is not protected.

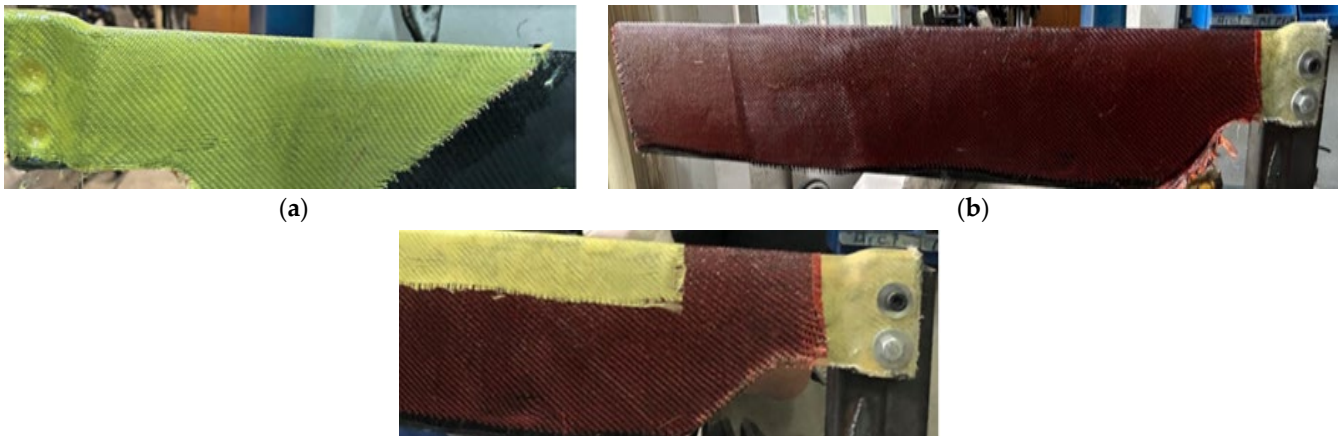

(**a**) (**b**) (**c**)

Figure 13. Blade manufacture. (**a**) Application of Kevlar coatings. (**b**) Application of carbon fibre coatings. (**c**) Application of Kevlar coatings to the leading edge of the blade.

The protection of the leading edge of the blade against damaging factors is provided by Kevlar fabric arranged in critical areas (Figure 13c). The main factors affecting blade performance, in general, are the following:

- Exposure to significant thermal variations can affect the structure of the material and lead to deformations or cracks in critical elements of the blade construction, such as the embedment area or the area of the strength girder box;
- Rainfall also represents a major risk due to icing, which can damage the anti-torque blade when the helicopter is flying in bad weather. They can become heavier and have a higher aerodynamic drag, which can lead to lower helicopter performance;
- Anti-torque blades are subject to stresses due to both aerodynamic and centrifugal forces. By performing a sufficiently large number of operating cycles, the strength structure fails due to material fatigue;

- Impact with foreign objects is a high risk because it manifests itself in two distinct aspects depending on the period of exposure. The first aspect refers to impact with relatively large objects, e.g., birds, power lines, etc., and results in blade deformation. The second aspect to be considered is sanding of the leading edge of the blade, which takes place over the entire life of the blade. Sanding occurs due to small impurities in the atmosphere that are entrained in the rotor disc formed by the blade when it is in operation.

Using the excellent abrasion and mechanical properties of Kevlar fibres, they are chosen to protect the blade's leading edge, which reduces the risks exposed above, while still managing to keep the mass of the blade low. After the polymerisation of the carbon and Kevlar layers added later, the surfaces are finished and polished. The blade is then ready for the final surface treatment, which is painting. For painting, the blade is degreased to prevent any impurities on the surface of the anti-torque blade from reaching the final layer. The shade applied to the surface to be painted is chosen from the RAL paint catalogue, which is the colour standard used in Europe and is referred to as RAL 6002 (Figure 14a). After the painting process, a third degreasing operation is applied to prepare the blade for the final coats of varnish. The varnish used is one varnish based on epoxy compounds and is called 1K acrylic varnish. After the two coats of varnish applied have dried, the blade is in the finished product stage (Figure 14b).

(**a**) (**b**)

Figure 14. Composite blade/ (**a**) Final blade shape manufactured using 3D-printed mould. (**b**) Detail of blade tip area.

5. Cost Evaluation

In this chapter, the manufacturing cost of the mould will be compared considering the two manufacturing options: 3D printing from PLA filament and CNC machining aluminium moulds. Also in this section, the cost and manufacturing time for the composite blade will be detailed starting from the two types of related costs: material costs and labour costs.

5.1. Economic Evaluation of Mould Manufacturing

Using the data centralised in Table 3, an analysis of the cost of manufacturing the mould by the additive manufacturing process using a 3D printer was carried out. Thus, approximately 9.3 kg PLA filament (approximately 13 rolls) were used, with each roll of material costing an average of EUR 44, which means that the material resources required for printing amount to EUR 572. The electricity used in 502 h of printing can be multiplied by the 500 Wh used by the Ultimaker S5 printer, giving a total of 251 kWh. Multiplying this value by the price of 0.3 EUR/kWh leads to the conclusion that the cost of printing associated with electricity consumption amounts to EUR 75.3. The last cost is the user labour cost. The labour is broken down as follows: pre-processing of the STL model and preparation of the printer—15 h; post-processing of the printed parts—2 h; assembly of the mould and adjustment of the active surfaces (materials included in the labour)—16 h; and application of the surface treatment (materials included in the labour)—5 h. Thus, the labour involved in making the prototype mould of the anti-torque blade was 38 h and

worth EUR 380. The cost of labour was calculated at 10 EUR/hour. From the cost analysis, it results that for the manufacture of the two moulds (lower mould-MAT-COMP V3-FEMALE and upper mould-MAT-COMP V3-MALE), the value of EUR 1027.3 was reached.

Using the same input geometry, a quotation was requested via the Xometry website for a 6082 aluminium alloy mould in order to be able to compare the cost of making the mould. The production cost using CNC machining for the MAT-COMP V3-FEMALE (lower mould) was EUR 1926.56 and for the MAT-COMP V3-MALE (upper mould) was EUR 1409.30. Thus, to manufacture the mould, made of 6082 aluminium alloy, using CNC machining the total cost was EUR 3335.3.

From the study of the cost of manufacturing the mould (by the two processes), it can be concluded that the production of the prototype mould of the anti-torque blade by conventional methods (CNC machining) is about three times higher compared to the cost of producing the mould by additive manufacturing using a 3D printer. In Table 4, the manufacturing costs of composite blades using the two types of manufacturing processes (additive manufacturing and CNC machining) are summarised. The costs of the 3D-printed mould include the following: cost of materials, cost of energy, and cost of mould assembly and preparation. The total 3D-printed mould manufacturing time includes the 3D printing time and mould assembly and preparation time.

Table 4. Comparison of cost and manufacturing time of different processes for manufacturing moulds.

Manufacturing Process	Mould Cost [EUR]	Mould Manufacturing Time [h]
3D printing	1027.3	540
CNC machining	3335.3	120

5.2. Economic Evaluation of Composite Blade Manufacturing

The costs related to the physical manufacture of the prototype of the anti-torque blade can be separated into two distinct categories: costs related to the materials used and costs related to the labour involved in its manufacture. Thus, the costs but also the type of materials involved in the manufacture of the blade are centralised in Table 5, which are necessary to manufacture the composite blade. It can be observed that the total amount of materials involved in making the blade is around EUR 680.

Table 5. The type and quantity of materials used in the manufacture of composite blades.

No.	Material	Unit	Quantity	Unit Price [EUR]	Price [EUR]
1.	Carbon fibre	[m^2]	7	42.6	298.2
2.	Red carbon fibre	[m^2]	2	48.6	97.2
3.	Fibreglass tape 50 mm	[mL]	62	0.3	22.5
4.	Kevlar fibre	[m^2]	2	46	92
5.	Epoxy resin and hardener	[L]	1	37.4	37.4
6.	Degreaser	[L]	2	6.4	12.8
7.	Protective gloves	[pcs]	1	15	15
8.	Wax	[pcs]	1	11.2	11.2
9.	Brush 0.5″	[pcs]	5	0.8	4
10.	Brush 1″	[ppc]	5	0.9	4.5
11.	Brush 2″	[pcs]	5	1.2	6
12.	Protection foil	[pcs]	1	5	5
13.	Metal bushing ID20	[pcs]	2	5	10
14.	3D-printed core	[pcs]	1	20	20
15.	Carbon rods	[pcs]	2	3.6	7.2
16.	Paper tape	[pcs]	3	1.2	3.6
17.	Spray 400 mL RAL 6002	[pcs]	2	9.4	18.8
18.	Spray 400 mL lac 1k	[pcs]	2	7.6	15.2
	TOTAL				680.6

The cost of labour was calculated at 10 EUR/hour, the same as for the labour involved in the execution of the mould. The main operations used in the manufacture of the anti-torque blade are as follows: mould preparation 2 h; composite layer design 2 h; manual cutting of layers 10 h; preparation of workspace 2 h; preparation of materials needed in the lamination process 1 h; lamination of the anti-torque blade 9 h (3 operators × 3 h); blade demoulding 3 h; blade adjustment after demoulding 2 h; lamination of final carbon and Kevlar layers 8 h; blade adjustment 1 h; preparation for painting the blade 2 h; painting the blade 1 h; and varnishing the blade 1 h. These cumulative activities total 44 labour hours, which means that the total labour costs of the composite blade were EUR 440. Adding the material costs to the labour costs results in a production cost of an anti-torque composite blade of EUR 1120.

In Table 6, the total production costs of the composite blade are summarised, which include the costs of preparing and manufacturing the mould and the costs of manufacturing the composite blade for the two following scenarios: the CNC machining mould and the 3D-printed mould.

Table 6. Total production costs.

Mould Manufacturing Process	Total Production Costs [EUR]	Manufacture of Mould [Percentage from the Total Production Cost]	Production of the Blade [Percentage from the Total Production Cost]
3D printing	2147.3	47.84%	52.16%
CNC machining	4553.3	75%	25%

6. Conclusions

In conclusion, the manufacture of moulds using 3D printing is feasible and is becoming increasingly popular in the aerospace industry. The aerospace industry has also integrated additive manufacturing processes from the conceptual design stage to the final use of parts. Both in aerospace and in the automotive industry, additive manufacturing processes are starting to be used for prototypes, spare parts, and moulds because of the advantages they offer. For the design of the composite blade mould, several functional and technological aspects of this aeronautical product have been considered. With the mould being a TDV, when starting the design phase of the manufacturing process it was important to know the role and the way the product would be used to accommodate aspects that dictate the technological process of manufacturing the blade and therefore the design of the mould.

Due to the fact that the anti-torque blade mould exceeds the 3D printing size of the Ultimaker S5 printer, a puzzle-like assembly method of sections that fit into the printing space and allow the resulting mould to be correctly and accurately assembled from individual sections was chosen. The sections were bonded together using a polyurethane adhesive, the main advantage being that as the adhesive cures, it also increases in volume, ensuring the tightness of the mould. The manufacture of the anti-torque blade started with the preparation of the elements that are part of it (manufacture of the 3D-printed core) and the preparation of the moulds (lower and upper). The 3D-printed blade core takes the place of a structure for which traditionally PVC foam or moltoprene is used. The advantage of a 3D-printed core is the creation of a hollow cavity, which reduces the overall mass of the aircraft product.

The labour involved in making the prototype blade mould was 38 h and amounts to EUR 380. The total investment results in a total cost for the manufacture of the two moulds (MAT-COMP V3-FEMALE and MAT-COMP V3-MALE) of EUR 1027.3. The labour involved in laminating the blade was EUR 440 and the materials used were EUR 680, totalling EUR 1120.

Thus, for the manufacture of the prototype of the anti-torque blade, the total production costs were EUR 2147.3, of which 47.84% of the amount was invested in the preparation of the manufacture and 52.16% of the amount was invested in the production of the product

(blade). This represents a major advance over conventional processes (CNC machining) where 75% of the amount is invested in the manufacturing preparation and the rest (25%) in the production of the product. At the same time, this type of 3D-printed mould has a limited lifetime and 15 to 30 blades can typically be manufactured. In conclusion, the feasibility of producing 3D-printed moulds in a short time and at a low cost compared to CNC machining aluminium moulds has been demonstrated.

Author Contributions: Conceptualization, R.T. and S.-M.Z.; methodology, R.T. and S.-M.Z.; software, R.T. and S.-M.Z.; validation, R.T. and S.-M.Z.; investigation, R.T. and S.-M.Z.; resources, R.T. and S.-M.Z.; data curation, R.T. and S.-M.Z.; writing—original draft preparation, R.T. and S.-M.Z.; writing—review and editing, R.T. and S.-M.Z.; visualization, R.T. and S.-M.Z.; supervision, R.T. and S.-M.Z.; project administration, R.T. and S.-M.Z.; funding acquisition, R.T. and S.-M.Z. All authors have read and agreed to the published version of the manuscript.

Funding: This research received no external funding.

Institutional Review Board Statement: Not applicable.

Informed Consent Statement: Not applicable.

Data Availability Statement: The raw data supporting the conclusions of this article will be made available by the authors on request.

Acknowledgments: We hereby acknowledge the Transilvania University of Brasov for providing the infrastructure used in this paper.

Conflicts of Interest: The authors declare no conflicts of interest.

References

1. Morozov, E.V.; Sylantiev, S.A.; Evseev, E.G. Impact damage tolerance of laminated composite helicopter blades. *Compos. Struct.* **2003**, *62*, 367–371. [CrossRef]
2. Roy, A.M. Finite Element Framework for Efficient Design of Three Dimensional Multicomponent Composite Helicopter Rotor Blade System. *Eng* **2021**, *2*, 69–79. [CrossRef]
3. Rasuo, B. Helicopter Tail Rotor Blade from Composite Materials: An Experience. *SAE Int. J. Aerosp.* **2011**, *4*, 828–838. [CrossRef]
4. Ahmad, K.; Baig, Y.; Rahman, H.; Hasham, H. Progressive failure analysis of helicopter rotor blade under aeroelastic loading. *Aviation* **2020**, *24*, 33–41. [CrossRef]
5. Lazăr, S.; Dobrotă, D.; Breaz, R.-E.; Racz, S.-G. Eco-Design of Polymer Matrix Composite Parts: A Review. *Polymers* **2023**, *15*, 3634. [CrossRef]
6. Barile, C.; Casavola, C.; Cililis, F.D. Mechanical comparison of new composite materials for aerospace applications. *Compos. Part B* **2019**, *162*, 122–128. [CrossRef]
7. Parveez, B.; Kittur, M.I.; Badruddin, I.A.; Kamangar, S.; Hussien, M.; Umarfarooq, M.A. Scientific Advancements in Composite Materials for Aircraft Applications: A Review. *Polymers* **2022**, *14*, 5007. [CrossRef]
8. Zaharia, S.M.; Martinescu, I. Management of accelerated reliability testing. *Teh. Vjesn.* **2016**, *23*, 1447–1455.
9. Zaharia, S.M. Reliability testing and failure analysis for spar structure of helicopter rotor blade. *Rev. Air Force Acad.* **2016**, *2*, 39–46. [CrossRef]
10. Rasuo, B. Experimental techniques for evaluation of fatigue characteristics of laminated constructions from composite materials: Full-scale testing of the helicopter rotor blades. *J. Test. Eval.* **2011**, *39*, 237–242.
11. Van der Ven, H.; Bakker, R.J.J.; van Tongeren, J.H.; Bos, M.J.; Münninghoff, N. A modelling framework for the calculation of structural loads for fatigue life prediction of helicopter airframe components. *Aerosp. Sci. Technol.* **2012**, *23*, 26–33. [CrossRef]
12. Shahani, A.R.; Mohammadi, S. Damage tolerance and classic fatigue life prediction of a helicopter main rotor blade. *Meccanica* **2016**, *51*, 1869–1886. [CrossRef]
13. Zuo, C.; Ma, J.; Wei, C.; Yue, T.; Song, J. Deformation Measurements of Helicopter Rotor Blades Using a Photogrammetric System. *Photonics* **2022**, *9*, 466. [CrossRef]
14. Balzarek, C.; Kalow, S.; Riemenschneider, J.; Rivero, A. Manufacturing and Testing of a Variable Chord Extension for Helicopter Rotor Blades. *Actuators* **2022**, *11*, 53. [CrossRef]
15. Debski, H.; Ostapiuk, M. Numerical FEM analysis for the part of composite helicopter rotor blade. *J. Kones* **2012**, *19*, 71–77. [CrossRef]
16. Filippi, M.; Zappino, E.; Carrera, E.; Castanie, B. Effective Static and Dynamic Finite Element Modeling of a Double Swept Composite Rotor Blade. *J. Am. Helicopter Soc.* **2020**, *65*, 1–12. [CrossRef]
17. Kliza, R.; Scislowski, K.; Siadkowska, K.; Padyjasek, J.; Wendeker, M. Strength analysis of a prototype composite helicopter rotor blade spar. *Appl. Comput. Sci.* **2022**, *18*, 5–19. [CrossRef]

18. Elfarra, M.A. Optimization of helicopter rotor blade performance by spline-based taper distribution using neural networks based on CFD solutions. *Eng. Appl. Comput. Fluid Mech.* **2019**, *13*, 833–848. [CrossRef]
19. Chakrapani, S.K.; Barnard, D.; Dayal, V. Nondestructive evaluation of helicopter rotor blades using guided Lamb modes. *Ultrasonics* **2014**, *54*, 826–833. [CrossRef]
20. Pawar, P.M.; Ganguli, R. Helicopter rotor health monitoring-A review. *Proc. Inst. Mech. Eng. Part G J. Aerosp. Eng.* **2007**, *221*, 631–647. [CrossRef]
21. Amura, M.; Aiello, L.; Colavita, M.; De Paolis, F.; Bernabei, M. Failure of a Helicopter Main Rotor Blade. *Procedia Mater. Sci.* **2014**, *3*, 726–731. [CrossRef]
22. Dos Santos, F.L.M.; Peeters, B.; Van der Auveraer, H.; Góes, L.C.S.; Desmet, W. Vibration-based damage detection for a composite helicopter main rotor blade. *Case Stud. Mech. Syst. Signal Process.* **2016**, *3*, 22–27. [CrossRef]
23. Tondini, F.; Basso, A.; Arinbjarnar, U.; Nielsen, C.V. The Performance of 3D Printed Polymer Tools in Sheet Metal Forming. *Metals* **2021**, *11*, 1256. [CrossRef]
24. Zelený, P.; Vána, T.; Stryal, J. Application of 3D printing for specific tools. *Mater. Sci Forum.* **2016**, *862*, 316–323. [CrossRef]
25. Sandhu, K.; Singh, G.; Singh, S.; Kumar, R.; Prakash, C.; Ramakrishna, S.; Królczyk, G.; Pruncu, C.I. Surface Characteristics of Machined Polystyrene with 3D Printed Thermoplastic Tool. *Materials* **2020**, *13*, 2729. [CrossRef]
26. Redwood, B.; Schöffer, B.; Garret, B. *The 3D Printing Handbook: Technologies, Design and Applications, 3D Hubs, B.V.*; Coers & Roest: Amsterdam, The Netherlands, 2017.
27. Zaharia, S.-M.; Pop, M.A.; Cosnita, M.; Croitoru, C.; Matei, S.; Spîrchez, C. Sound Absorption Performance and Mechanical Properties of the 3D-Printed Bio-Degradable Panels. *Polymers* **2023**, *15*, 3695. [CrossRef] [PubMed]
28. Krause, J.; Bhounsule, P. A 3D Printed Linear Pneumatic Actuator for Position, Force and Impedance Control. *Actuators* **2018**, *7*, 24. [CrossRef]
29. Ozcelik, A. 3D Printed Device for Separation of Cells and Particles by Tilted Bulk Acoustic Wave Actuation. *Actuators* **2022**, *11*, 249. [CrossRef]
30. Hong, F.; Tendera, L.; Myant, C.; Boyle, D. Vacuum-Formed 3D Printed Electronics: Fabrication of Thin, Rigid and Free-Form Interactive Surfaces. *SN Comput. Sci.* **2022**, *3*, 275. [CrossRef]
31. Modi, Y.K. Calcium sulphate based 3D printed tooling for vacuum forming of medical devices: An experimental evaluation. *Mater. Technol.* **2018**, *33*, 642–650. [CrossRef]
32. Kuo, C.-C.; Tasi, Q.-Z.; Hunag, S.-H.; Tseng, S.-F. Development of an Injection Mold with High Energy Efficiency of Vulcanization for Liquid Silicone Rubber Injection Molding of the Fisheye Optical Lens. *Polymers* **2023**, *15*, 2869. [CrossRef] [PubMed]
33. Habrman, M.; Chval, Z.; Ráž, K.; Kučerová, L.; Hůla, F. Injection Moulding into 3D-Printed Plastic Inserts Produced Using the Multi Jet Fusion Method. *Materials* **2023**, *16*, 4747. [CrossRef] [PubMed]
34. Ian Gibson, I.G. *Additive Manufacturing Technologies 3D Printing, Rapid Prototyping, and Direct Digital Manufacturing*; Springer: Berlin/Heidelberg, Germany, 2015.
35. Tondini, F.; Arinbjarnar, U.; Basso, A.; Nielsen, C.V. 3D printing to facilitate flexible sheet metal forming production. *Procedia CIRP* **2021**, *103*, 91–96. [CrossRef]
36. Pujante, J.; González, B.; Garcia-Llamas, E. Pilot Demonstration of Hot Sheet Metal Forming Using 3D Printed Dies. *Materials* **2021**, *14*, 5695. [CrossRef] [PubMed]
37. Zaragosa, V.G.; Strano, M.; Iorio, L.; Monno, M. Sheet metal bending with flexible tools. *Proc. Manuf.* **2019**, *29*, 232–239. [CrossRef]
38. Yi, C.; Jiang, L.; Qing, G.; Lei, W. 3D printing of CF/nylon composite mold for CF/epoxy parabolic antenna. *J. Eng. Fibers Fabr.* **2020**, *15*, 1558925020969484.
39. Bianchi, I.; Gentili, S.; Greco, L.; Mancia, T.; Simoncini, M.; Vita, A. 3D printed molds for manufacturing of CFRP components. *Procedia CIRP* **2023**, *118*, 816–821. [CrossRef]
40. Russo, A.C.; Andreassi, G.; di Girolamo, A.; Pappada, S.; Buccoliero, G.; Barile, G.; Vegliò, F.; Sotornelli, V. FDM 3D Printing of high performance composite materials. In Proceedings of the Workshop on Metrology for Industry 4.0 and IoT, Naples, Italy, 4–6 June 2019.
41. Kumar, V.; Alwekar, S.P.; Kunc, V.; Cakmak, E.; Kishore, V.; Smith, T.; Lindahl, J.; Vaidya, U.; Blue, C.; Theodore, M.; et al. High-performance molded composites using additively manufactured preforms with controlled fiber and pore morphology. *Addit. Manuf.* **2021**, *37*, 101733. [CrossRef]
42. Hadăr, A.; Voicu, A.-D.; Baciu, F.; Vlăsceanu, D.; Tudose, D.-I.; Pastramă, Ş.-D. A Novel Composite Helicopter Tail Rotor Blade with Enhanced Mechanical Properties. *Aerospace* **2023**, *10*, 647. [CrossRef]
43. Dippenaar, D.J.; Schreve, K. 3D printed tooling for vacuum-assisted resin transfer moulding. *Int. J. Adv. Manuf. Technol.* **2013**, *64*, 755–767. [CrossRef]
44. Aerospace Manufacturing. Available online: https://www.aero-mag.com/thermwood-and-bell-3d-print-helicopter-blade-mould/ (accessed on 30 September 2023).
45. Post, B.K.; Richardson, B.; Lind, R.; Love, L.J.; Lloyd, P.; Kunc, V.; Rhyne, B.J.; Roschli, A.; Hannan, J.; Nolet, S.; et al. Big Area Additive Manufacturing Application in Wind Turbine Molds. In Proceedings of the 28th Annual International Solid Freeform Fabrication Symposium—An Additive Manufacturing Conference, SFF 2017, Austin, TX, USA, 7–9 August 2017; pp. 2430–2446.
46. Euler, A.H.L.; Beziac, G.F.A. Method of Manufacturing a Helicopter Rotor Blade. U.S. Patent 4,298,417, 3 November 1981.

47. Sutton, D.A.; Wasikowski, M.E.; Maresh, A.R.; Phillips, N.B. Adaptable Rotor Blade Design for Performance Flexibility. European Patent 10,807,705, 20 October 2020.
48. Fischer, J.M. *Handbook of Molded Part Shrinkage and Warpage*; William Andrew: Amsterdam, The Netherlands, 2013; ISBN 1455730572.
49. Hopmann, C.; Gerads, J.; Hohlweck, T. Investigation of an inverse thermal injection mould design methodology in dependence of the part geometry. *Int. J. Mater. Form.* **2021**, *14*, 209–321. [CrossRef]
50. Ageyeva, T.; Horváth, S.; Kovács, J.G. In-Mold Sensors for Injection Molding: On the Way to Industry 4.0. *Sensors* **2019**, *19*, 3551. [CrossRef] [PubMed]
51. Van der Borg, G.; Warner, H.; Ioannidis, M.; van den Bogaart, G.; Roos, W.H. PLA 3D Printing as a Straightforward and Versatile Fabrication Method for PDMS Molds. *Polymers* **2023**, *15*, 1498. [CrossRef] [PubMed]
52. Pop, M.A.; Cosnita, M.; Croitoru, C.; Zaharia, S.M.; Matei, S.; Spîrchez, C. 3D-Printed PLA Molds for Natural Composites: Mechanical Properties of Green Wax-Based Composites. *Polymers* **2023**, *15*, 2487. [CrossRef] [PubMed]
53. Youn, J.; Cho, M.; Chae, H.; Jeong, K.; Kim, S.; Do, S.; Lee, D. Development of Free-Form Assembly-Type Mold Production Technology Using 3D Printing Technology. *Buildings* **2023**, *13*, 2197. [CrossRef]
54. Joseph, T.M.; Kallingal, A.; Suresh, A.M.; Mahapatra, D.K.; Hasanin, M.S.; Haponiuk, J.; Thomas, S. 3D Printing of Polylactic Acid: Recent Advances and Opportunities. *Int. J. Adv. Manuf. Technol.* **2023**, *125*, 1015–1035. [CrossRef]
55. Hidalgo-Carvajal, D.; Muñoz, Á.H.; Garrido-González, J.J.; Carrasco-Gallego, R.; Alcázar Montero, V. Recycled PLA for 3D Printing: A Comparison of Recycled PLA Filaments from Waste of Different Origins after Repeated Cycles of Extrusion. *Polymers* **2023**, *15*, 3651. [CrossRef]
56. Ahmad, S.; Zhang, J.; Feng, P.; Yu, D.; Wu, Z.; Ke, M. Processing technologies for Nomex honeycomb composites (NHCs): A critical review. *Compos. Struct.* **2020**, *250*, 112545. [CrossRef]
57. Atas, C.; Sevim, C. On the impact response of sandwich composites with cores of balsa wood and PVC foam. *Compos. Struct.* **2010**, *93*, 40–48. [CrossRef]
58. Castro Composites. Technical Data Sheet for TC203T Carbon Fiber. Available online: https://www.castrocompositesshop.com/en/fibre-reinforcements/2371-200-gm2-3k-carbon-fabric-twill-2x2-100-cm-width-8431252547043.html (accessed on 23 November 2023).
59. East Coast Fibreglass Supplies. Technical Data Sheet for Fibreglass Tape—200 G × 50 mm. Available online: https://www.ecfibreglasssupplies.co.uk/fibreglass-tape-200g-x-50mm (accessed on 23 November 2023).
60. Easy Composites Ltd. Technical Data Sheet for Kevlar®Fabric. Available online: https://media.easycomposites.eu/datasheets/EC-TDS-300g-Twill-Weave-Kevlar-Cloth.pdf (accessed on 23 November 2023).
61. Easy Composites Ltd. Technical Data Sheet EL2 Epoxy Laminating Resin. Available online: https://media.easycomposites.eu/datasheets/EC-TDS-EL2-Epoxy-Laminating-Resin.pdf (accessed on 23 November 2023).
62. Easy Composites Ltd. Technical Data Sheet for AT30 Epoxy Hardener. Available online: https://www.easycomposites.co.uk/at30-epoxy-resin-hardener-fast-or-slow (accessed on 23 November 2023).
63. Easy Composites Ltd. Technical Data Sheet for Red 2 × 2 Twill 3k Carbon Fibre. Available online: https://media.easycomposites.eu/datasheets/Pyrofil-TRSeries.pdf (accessed on 23 November 2023).